Journal of Geophysical Research – Solid Earth

Supporting Information for

Inverse migration of seismicity quiescence during the 2019 Ridgecrest sequence

David Marsan [1], Zachary E. Ross [2]

[1] Université Savoie Mont-Blanc, CNRS, IRD, IFSTTAR, Isterre, 73376 Le Bourget-du-Lac, France.

[2] Seismological Laboratory, California Institute of Technology, Pasadena, CA 91125, USA.

Contents of this file

Introduction

We here provide three sections, that develop on the analyses proposed in the main text:

- Text S1, Table S1, Figures S1 – S9 reproduce the same analysis but using the SCSN rather than the QTM dataset.

- Text S2, Figure S10 detail how the earthquake rate can be corrected for undetected events

- Text S3, Figures S11 – S14 quantify the accuracy ad robustness of the method by using synthetic datasets.

Text S1 – Analysis without the QTM detections

We iterate the same analysis as in the main text, but this time only using the SCSN catalog. The dataset is made of 18200 earthquakes (from the M6.4 mainshock to 18.86 days past the M7.1 mainshock), occurring at a roughly constant rate of 1410 earthquake/day up to 7 days after the M7.1 mainshock, at which time the rate drops by a factor of 2.5. We therefore initially limit this analysis to the 8.4 days after the M6.4 mainshock, cf. Figure S1. The rate is equivalent to 1 earthquake occurring every 61 s on average. We note that this rate fluctuates about twice as much as the complete catalog (SCSN + QTM earthquakes) does, and for a shorter time interval (8.4 days compared to about 20 days), see Figure S1, making this analysis more prone to estimation errors.

The smoothed magnitudes decay with the logarithm of time according to $\bar{m}_{mod}(t) = -0.41 \ln(t) + 1.49$ for the M6.4 sequence (t is time in days after the M6.4), and $\bar{m}_{mod}(t) = -0.47 \ln(t) + 2.08$ for the M7.1 sequence (t is time in days after the M7.1), cf. Figure S2, hence about 0.6 to 0.7 larger than with the QTM catalog. Given those models, we then fit the distribution of magnitude increments $\delta m_i = m_i - \bar{m}_{mod}(t_i)$ with a Gutenberg-Richter law modulated by a Gumbel detection function, cf. Figure S3. We find that b=1.10, and μ=-0.19 corresponding to a mean δm of 0.03. The detection probabilities q corresponding to the best Gumbel model are roughly distributed according to a uniform law, albeit with some variability, see Figure S4.

We compute the change of rate caused by the M7.1 mainshock by taking the 100 closest neighbours (earthquakes occurring between the two mainshocks), using a model that accounts for both the M6.4 mainshock and its M5.3 aftershock, and estimating the rate change for the 7 days after the M7.1 mainshock. The maps of the rate change (in log 10 scale) and normalized variance of the model are shown in Figure S5, along with the rate vs time graphs for the 6 selected locations (Figure S6); the ρ and v values of these 6 locations are summarized in Table A1, and compared to the values obtained using the QTM earthquakes as well.

The main difference between the two analyses is the absence of a seismicity quiescence near the north-eastern tip of the cross-cut (SWV) fault (location B), which existence is supported by the Coulomb stress change model. This quiescence, as far as we can tell from our analysis, is instantaneous when considering the QTM dataset, so the fact that we here study a shorter, 7 day-long target period is not responsible for this difference. We further investigate the activity close to location B by selecting all the $m \geq 2$ earthquakes (SCSN and QTM) within 2 km of B, and compute their occurrence rates in the estimated $m \geq 2$ complete periods (that can be inferred directly from Figure 3). We then find that this area is indeed characterized by quiescence, but significantly milder than the one of Figure 6 (ρ=-0.23), cf. Figure S8. As described in Text S3, this direct approach is particularly prone to estimation errors, and this estimated ρ value must therefore be considered as only a rough estimate.

We finally checked that the shutdown observed for the cross-cut M6.4 fault is present over a longer time period. We use the SCSN catalog up to 26/5/2020, and select $m \geq 2$ earhquakes that are less than 300 m away (hypocenter distances) from any repeating earthquake of the QTM dataset that had occurred before the M7.1 mainshock. For the SCSN catalog, completeness at $m \geq 2$ requires removing the first 0.35 days after the M6.4 mainshock and the first 2 days after the M7.1 shock (same as in Figure S8). We superpose in Figure S9 the obtained rates to the rates of Figure 8; a correction factor of $10^{0.92*3}=575$ (since b=0.92 for this sequence) is applied to account for the difference in magnitudes between the two rates. The $m \geq 2$ rate continues to decay the same way over 10 months as it did for over 18 days. The major difference is that the pre-M7.1 rate cannot be well resolved with the SCSN data alone: this rate does not appear to decay, due to the limited time interval over which the data is complete at $m \geq 2$. This would normally prevent extrapolating the M6.4 aftershock rate to longer times, and therefore would also prevent any meaningful estimation of the change in rate due to the M7.1 shock, demonstrating again the gain brought by using a refined catalog for this type of analysis.

Text S2 – Rate correction

We first recall our working hypothesis that an earthquake is detected if there are no earthquakes with a larger magnitude within a (screening) time Δt prior to it. This model was already proposed by Hainzl (2016a), who also showed that it can explain why the completeness magnitude decays with the logarithm of time during aftershock sequences. We here demonstrate that the detection probability q follows a Gumbel law, and then derive the normalization π that allows to correct the observed rate for missing earthquakes.

For n earthquakes with magnitudes $\{m_1, m_2, \ldots, m_n\}$ independently drawn from a Gutenberg-Richter law with exponent β and minimum magnitude m_0 , the maximum magnitude M has a density $f_M(M)=n\beta e^{-\beta(M-m_0)}\left(1-e^{-\beta(M-m_0)}\right)^{n-1}$. Assuming that the observed magnitudes are always much greater than the physically-controlled minimum magnitude m_0 , hence $n \gg 1$, this density can be rewritten as $f_M(M)=n\beta e^{-\beta(M-m_0)}e^{-ne^{-\beta(M-m_0)}}$. This corresponds to a Gutenberg-Richter law modulated by a detection probability $q(m)=e^{-ne^{-\beta(m-m_0)}}$ which we rewrite as $q(m)=e^{-e^{-\beta(m-\mu)}}$, with $\mu=m_0+\frac{1}{\beta}\ln(n)$. This parameter μ cannot be inferred a priori since neither m_0 nor n are known. However, the mean $\bar{M}=\int_{m_0}^{\infty} f_M(M)M$ can be shown to be equal to $\frac{1}{\beta}\left(1+\frac{1}{2}+\frac{1}{3}+\ldots+\frac{1}{n}\right)+m_0$, which, in the limit $n \gg 1$, can be approximated as $\bar{M}=m_0+\frac{1}{\beta}(\ln(n)+0.577)$ or, equivalently, to $\bar{M}=\mu+\frac{0.577}{\beta}$. We therefore simply obtain an empirical

estimate of μ by subtracting $0.577/\beta$ to the average of the observed magnitudes *M*.

Given that *q* follows a Gumbel law, we can deduce the threshold magnitude m_p for which the $m>m_p$ earthquakes are detected with probability *p*. It comes that $m_p=\mu-\frac{1}{\beta}\ln(\ln\frac{1}{p})$. For $p=0.9$, this gives $m_p=\mu+\frac{2.25}{\beta}$, which can be used as a proxy for the magnitude of completeness.

We now search how to estimate the real rate of earthquakes above a fixed magnitude m_{min} , which is a priori different from the (unknown) physical limit m_0 . This rate includes the observed earthquakes, but also the ones that were not detected. At time *t*, the incremental magnitudes $\delta m_i=m_i-\bar{m}_{mod}(t)$ are distributed according to a Gutenberg-Richter law multiplied by a Gumbel detection probability $q(\delta m)=e^{-e^{-\beta(\delta m-\mu)}}$, with the two parameters β and $\mu=\overline{\delta m}-\frac{0.577}{\beta}$ independent of time. We recall that $\bar{m}_{mod}(t)$ is the modeled mean magnitude at time *t*, which is described in Section 3.1. The probability to detect an earthquake with a magnitude known to be greater than m_{min} is therefore $\pi=\int_{m_{min}}^{\infty} dm\beta e^{-\beta(m-m_{min})}e^{-e^{-\beta(m-m_{mod}-\mu)}}$, i.e., the mean of $q(\delta m)$. After some algebra, we obtain that $\pi=e^{-\beta(\mu+\bar{m}_{mod}-m_{min})}\times\{1-e^{-e^{\beta(\mu+m_{mod}-m_{min})}}\}$. The maximum likelihood estimate of the real rate is then $\lambda(t)=\frac{\lambda_{obs}(t)}{\pi(t)}$, where the observed rate λ_{obs} and the probability π are calculated for a fixed minimum magnitude m_{min} (i.e., we only count $m>m_{min}$ earthquakes in the observed rate). Hainzl (2016b) already proposed a similar correction (his equation 3), albeit without formulating it with a Gumbel probability of detection. We further note that, in the limit $\bar{m}_{mod}\gg m_{min}$, which is true when the observed magnitudes are much greater than m_{min} , π reduces to $\pi=e^{-\beta(\mu+\bar{m}_{mod}-m_{min})}$ which is simply proportional to $e^{-\beta m_c}$; this was used by Peng et al. (2007) to correct for undetected earthquakes at early times in aftershock sequences.

We test this correction on a synthetic catalog with $m\geq-1$ earthquakes generated by an ETAS model with zero background rate, following a mainshock of magnitude 7, and taking realistic model parameters (p=1, c=1 s, productivity parameter $\alpha=2$, $\beta=2.14$). The aftershock sequence is computed for 7 days, at which time the rate of $m\geq-1$ earthquakes is 9223 per day, hence one earthquake every 9.4 s on average. We then discard (as undetected) all earthquakes that are preceded within 20 s by a larger earthquake, which reduces the dataset to 30890 out of 810593 (3.8%). The observed rate of detected earthquakes is then roughly constant, equal to 4412 earthquakes per day on average (or one earthquake every 19.5 s on average). After smoothing the magnitudes, we obtain a best-fit model $\bar{m}_{mod}(t)=-0.42\ln(t)+0.64$ (Figure S10a), and define the magnitude increments $\delta m_i=m_i-\bar{m}_{mod}(t_i)$, which are distributed according to a

Gutenberg-Richter law with estimated $\beta=2.05$ (in place of the "true" 2.14 value) modulated by a Gumbel detection probability (Figure S10b). We then infer the "true" rate of $m\geq -1$ earthquakes based on the detected dataset only, see Figure S10c. The agreement with the true rate is overall very good, except at times when a large aftershock occurs and causes the rate to increase over a short period of time; these transient increases are missed by our method because we fit the smoothed magnitudes with a simple, log-linear model $\bar{m}_{mod}(t)$. More variable models that can accommodate transient increases would be needed to better fit the true rate. A simple alternative is provided by taking $\bar{m}_{mod}(t)$ to simply following the smoothed magnitudes, which better model these transient changes (Figure S10d). This is however not a viable option if the final goal is to extrapolate the estimated rate to later times in order to compute rate changes, as we do in this study, because we need a parameterized rate model to perform this extrapolation.

We finally demonstrate that in our model the $q_i=q(\delta m_i)=q(m_i-\bar{m}_{mod}(t_i))$ values are uniformly distributed. Given an initial set $\{m_i\}$ of magnitudes (before the detection filter) with density $f_m(m)=\beta e^{-\beta(m_i)}$, and the Gumbel detection probability $q(m)=e^{-e^{-\beta(m-\mu)}}$, we define the observed (i.e., after the detection filter) magnitudes as $\{x_i\}$, hence with density $f_x(x)=f_m(x)q(x)\frac{e^{\beta(\mu-m_0)}}{1-e^{-e^{\beta(\mu-m_0)}}}$, where the last fraction is just a normalization factor. The question is then: how are the remaining q_i values distributed after the detection filter? Denoting $f_q(q)$ the corresponding density, $f_x(x)dx=f_q(q)dq$ yields that $f_q(q)=\frac{1}{1-e^{-e^{\beta(\mu-m_0)}}}$, hence a constant value. The distribution is thus uniform between $q=e^{-e^{-\beta(m_0-\mu)}}$ (for $x=m_0$) and 1. Since the q_i values can be computed from the observed magnitudes, this can serve as a way to assess whether the model is consistent with the data.

Text S3 – Synthetics and tests

We here test the accuracy and robustness of the rate change estimation. To do this, we simulate synthetic sets of earthquakes with a known, imposed rate change at the time of the 2nd mainshock, trim them according to a detection ("screening") filter, and then apply our procedure as described in section 3 to compare the estimated rate change to the true one.

The synthetic dataset is made up of two subsets: (1) a "local" dataset, which corresponds to the area for which the rate change is estimated, and (2) a "global" dataset which corresponds to all the earthquakes (including the local ones), which is used to thin the catalogs, hence simulating the lack of detection due to large earthquakes screening smaller ones. We run the simulation up to t=20 days. Both datasets are drawn using a purely temporal ETAS model with no background rate: the earthquake rate is modeled as

$\lambda(t)=\sum_{t_i<t} K e^{\alpha m_i}(t+c-t_i)^{-p}$, with $\alpha=2$, $p=1$, $c=10^{-5}$ days. The magnitudes are drawn from a Gutenberg-Richter law with a b-value of 0.93 (as found for the QTM dataset), with minimum magnitude -1 and maximum magnitude 6.4. For the local dataset, we take $K=0.02$, and simulate the local direct aftershocks of the M6.4 mainshock with an Omori's law $\lambda_{M6.4}(t)=400(t+c)^{-1}$, which would be equivalent to the aftershock sequence of a m=4.95 mainshock (this "apparent" magnitude is less than 6.4 because we ought to simulate this sequence in a small zone, i.e., smaller than the whole rupture zone of a M6.4 mainshock). The rate $\lambda_{M6.4}(t)$ is multiplied by a factor 10^{ρ_0} at t=1.4 days, to simulate the local rate change (either triggering for $\rho_0>0$ or inhibition for $\rho_0<0$) due to the M7.1 mainshock. Once this direct sequence is generated, we then use the ETAS model to simulate local indirect aftershocks (i.e., aftershocks of aftershocks).

The global dataset is the collection of both the local dataset and a bigger dataset generated with the same ETAS model, but now with $K=0.13$, and imposing a m=6.4 mainshock at t=0 and a m=7.1 mainshock at t=1.4 days so to mimic the Ridgecrest sequence. We then discard all earthquakes that are preceded within 20 s by a larger earthquake. We show in Figure S11 a realization of such a simulation, for $\rho_0=0$ (no local rate change at the time of the M7.1). Due to the increased activity after t=1.4 days, the probability of detection is lowered, resulting in an apparent sharp shut-down of the local activity even though the true rate change is zero, while the global detected rate stays constant over the 20 days (Figure S11).

Running our analysis on this catalog, we find that $b=0.92$ (instead of the true 0.93 value), which allow us to correct the observed rates for the time-variable detection, see Figure S12. The inferred rate change is $\rho=0.09$ (i.e., a 25% increase of activity), which is mainly due to the fact that the imposed zero-rate change only applies to direct aftershocks of the M6.4 mainshock, but not to its secondary aftershocks. The latter produces extra activity that cause random-like fluctuations of the rate. We note that the estimated rate change on the full local catalog, i.e., before filtering with the time-varying detection, is $\rho=0.13$, which indeed directly measures the rate change caused by these secondary aftershocks. These random fluctuations effectively limit the resolution of the rate change.

To evaluate the accuracy of this method, we compare it to a direct attempt at estimating the rate change that would consist in (1) computing a completeness magnitude for the local catalog; we find that $m_c=0$ and $b=0.62$ give a good fit to the data (Figure S13). This b-value is clearly under-estimated, as already discussed in Hainzl (2017). (2) Selecting only $m\geq m_c$ earthquakes, yielding a set of 251 local earthquakes (out of the 536 detected). (3) Computing the rate and the associated rate change of this selected subset, see Figure S13. The quality of the fit is notably poor, and, more importantly, the estimated rate change is significantly under-estimated ($\rho=-0.94$ while the true ρ is 0).

We finally run 100 simulations, with ρ_0 varying between -1 and 1, and compare the estimated ρ values (using our method) with the true ones, cf. Figure S14. The correlation coefficient between the true and estimated ρ is 0.95, and the standard deviation of the residuals is 0.19, which gives an estimate of the uncertainty for a local subset of about detected 200 earthquakes in the first 1.4 days of the sequence, on average.

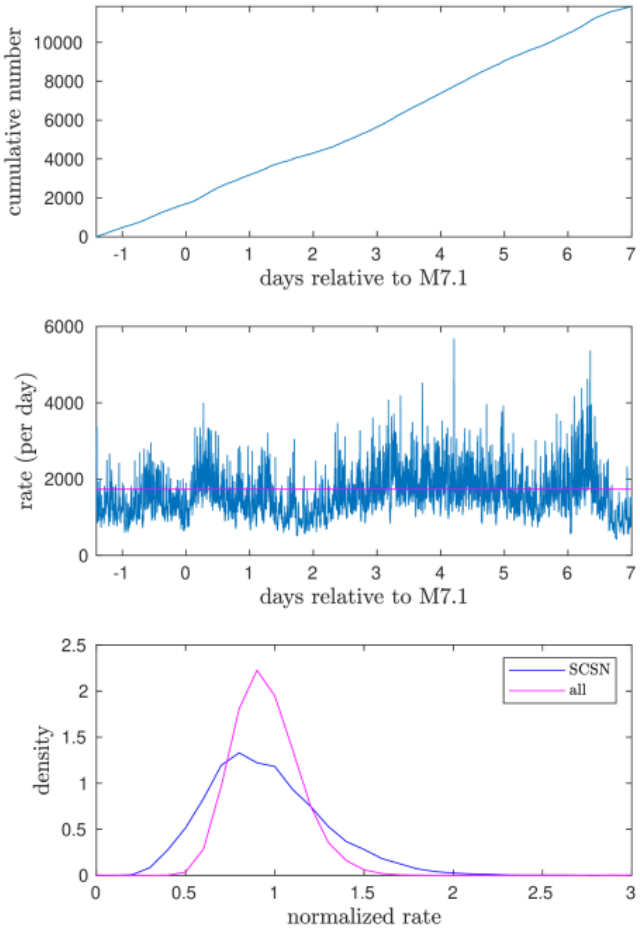

Figure S1: (top) cumulative number and (center) rate of earthquakes in the SCSN catalog (no QTM earthquakes) up to 7 days after the M7.1 mainshock. The magenta line gives the mean rate of 1410 earthquakes / day. (Bottom) rate of earthquakes normalized by the mean rate, for (blue) 8.4 days of the SCSN catalog (from the M6.4 mainshock to 7 days after the M7.1 mainshock), and for (magenta) the complete dataset, including both the SCSN and the QTM earthquakes, for 20 days (from the M6.4 mainshock up to 18.8 days after the M7.1 mainshock). The coefficient of variation (standard deviation divided by the mean) is 0.32 for just the SCSN data, and 0.18 for the whole catalog.

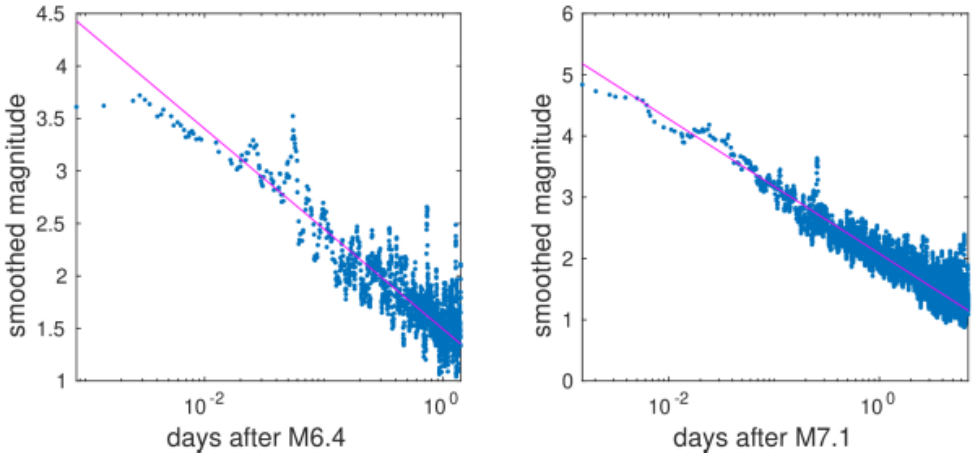

Figure S2: smoothed magnitude vs time, following each mainshock. The magenta lines show the best log-linear fits, see text.

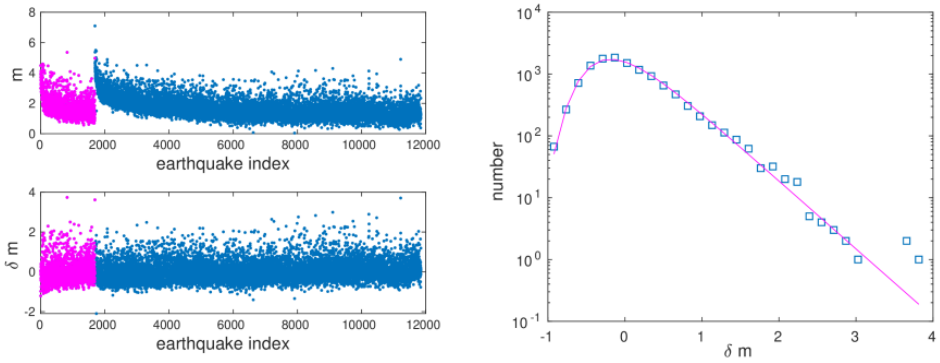

Figure S3: (top left) magnitude (m) and (bottom left) magnitude increment (δm) vs earthquake index. The magenta earthquakes are those occurring before the M7.1 mainshock. (Right) distribution of dm for the whole sequence, and best fit in magenta.

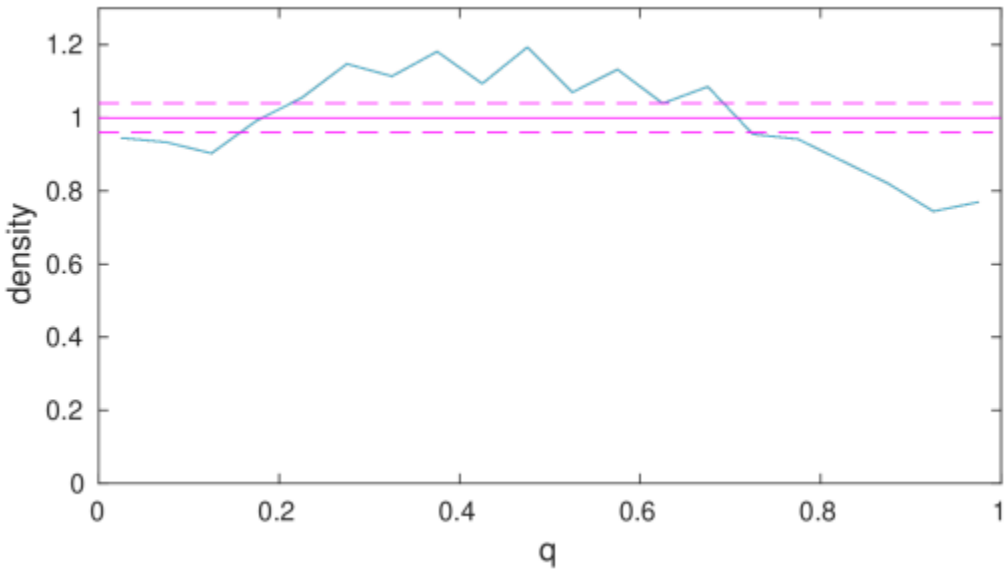

Figure S4: distribution of the detection probabilities q. The magenta line shows the uniform density that would be expected if the Gumbel detection model were perfect. The random fluctuations (in the case of a perfect model) would have a standard deviation of 0.04 (dashed lines).

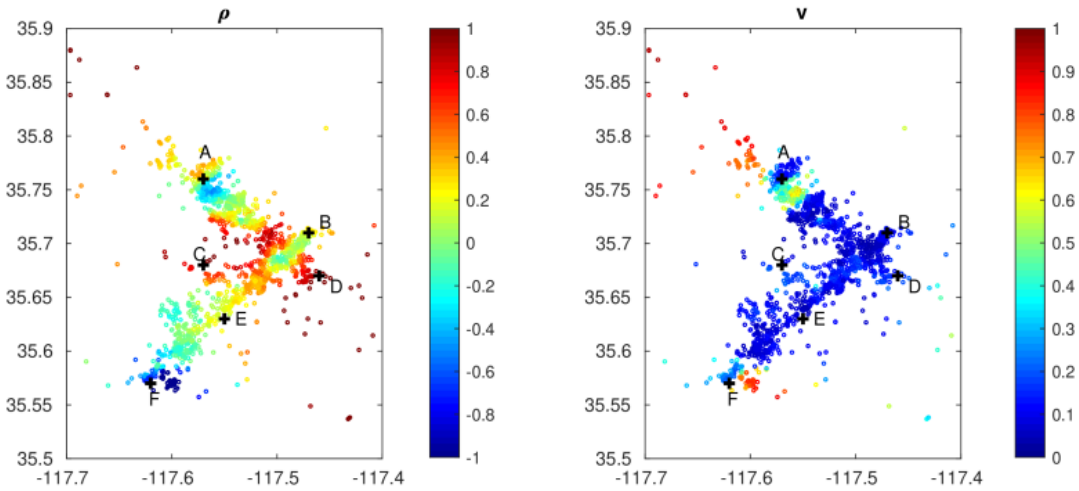

Figure S5: rate change ρ (in log 10 scale) and normalized variance v for the SCSN data without the QTM earthquakes, for 0 – 7 days after the M7.1 mainshock. Locations A to F are shown in Figure S6.

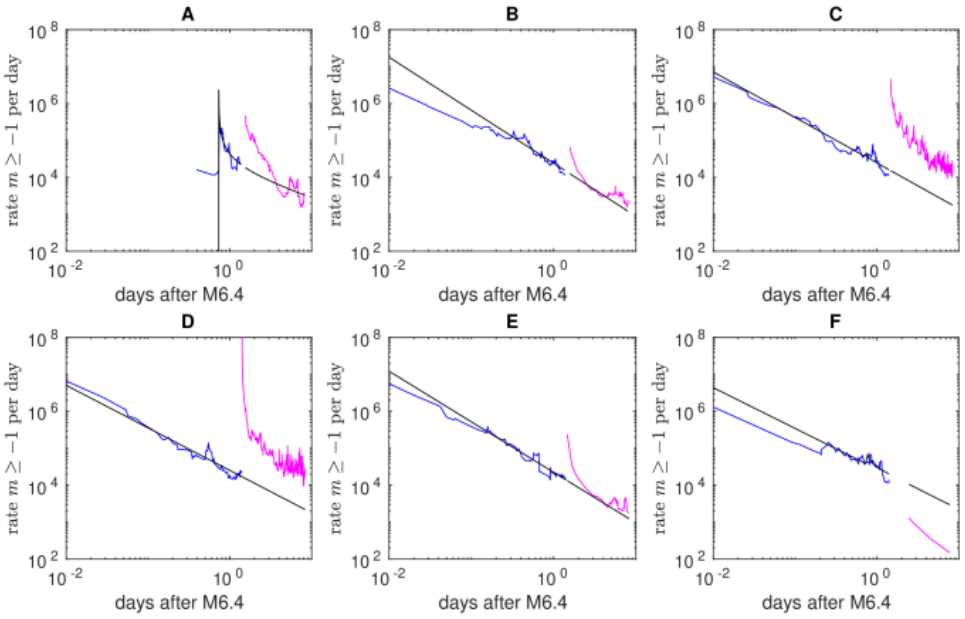

Figure S6: rate vs time for the 6 locations A – F of Figure S5. Blue : corrected rate for earthquakes occurring between the two M6.4 and M7.1 mainshocks. Magenta: corrected rate for earthquakes occurring after the M7.1 mainshock. Black: best fit to the blue curve, then extrapolated to the time interval after the M7.1 mainshock. This extrapolated rate, which is our best prediction, is then compared to the actual rate (in magenta).

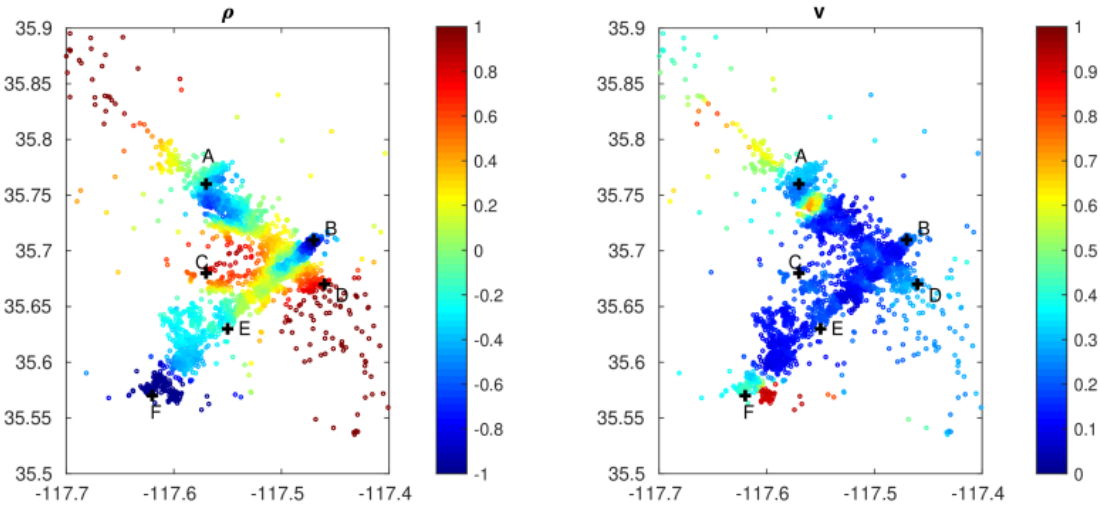

Figure S7: as with Figure S5, but including the QTM earthquakes as well, for the 0-7 days target period following the M7.1 mainshock. The smoothing is done on 400-earthquake disks (rather than 100).

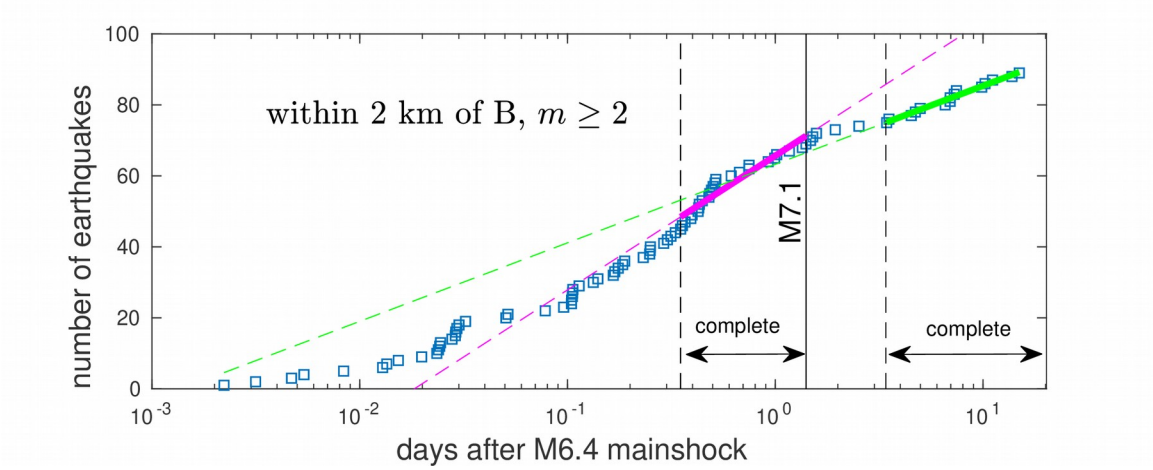

Figure S8: cumulative number of $m \geq 2$ earthquakes within 2 km of B (no depth selection). The magnitude of completeness is estimated to be less than 2 after 0.35 days after the M6.4 mainshock, and after 2 days after the M7.1 mainshock; the corresponding periods are outlined as "complete". The best log-linear fits for the two complete periods are shown in thick lines, and extrapolated to the whole time interval in dashed lines. The observed decrease in rate is by a factor of 1.7, equivalent to $\rho = -0.23$.

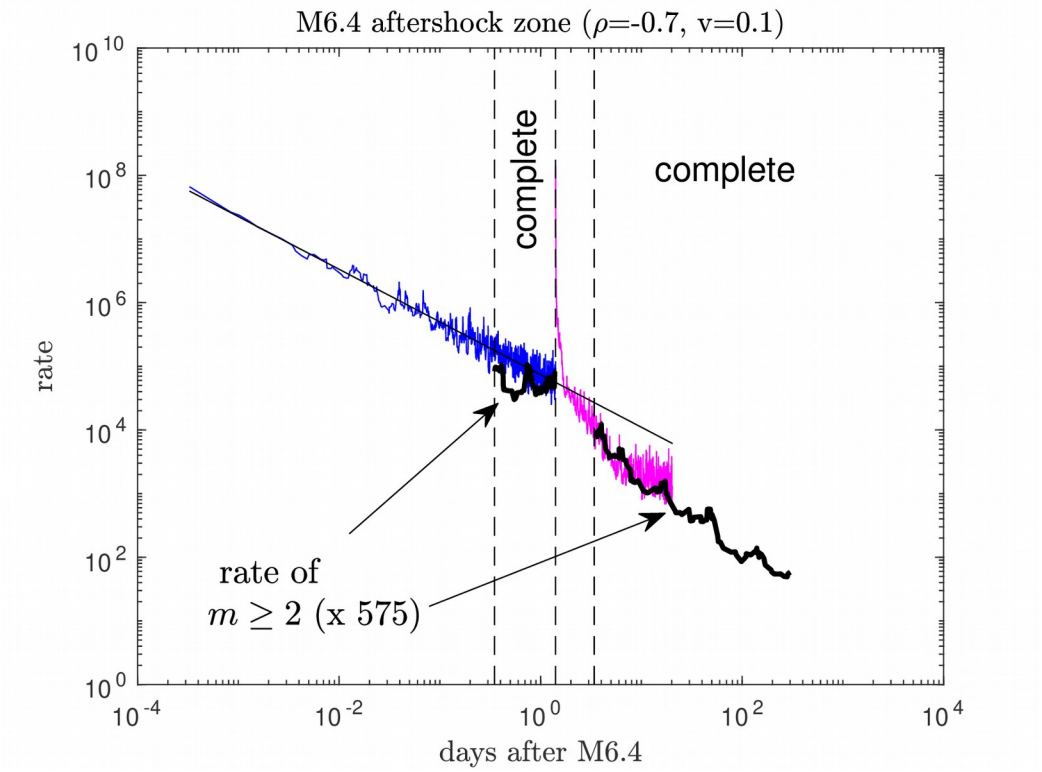

Figure S9: same as Figure 8, adding $m \geq 2$ earthquakes in the SCSN catalog up to 26/5/2020 (black curves). The complete periods (at $m \geq 2$) are indicated.

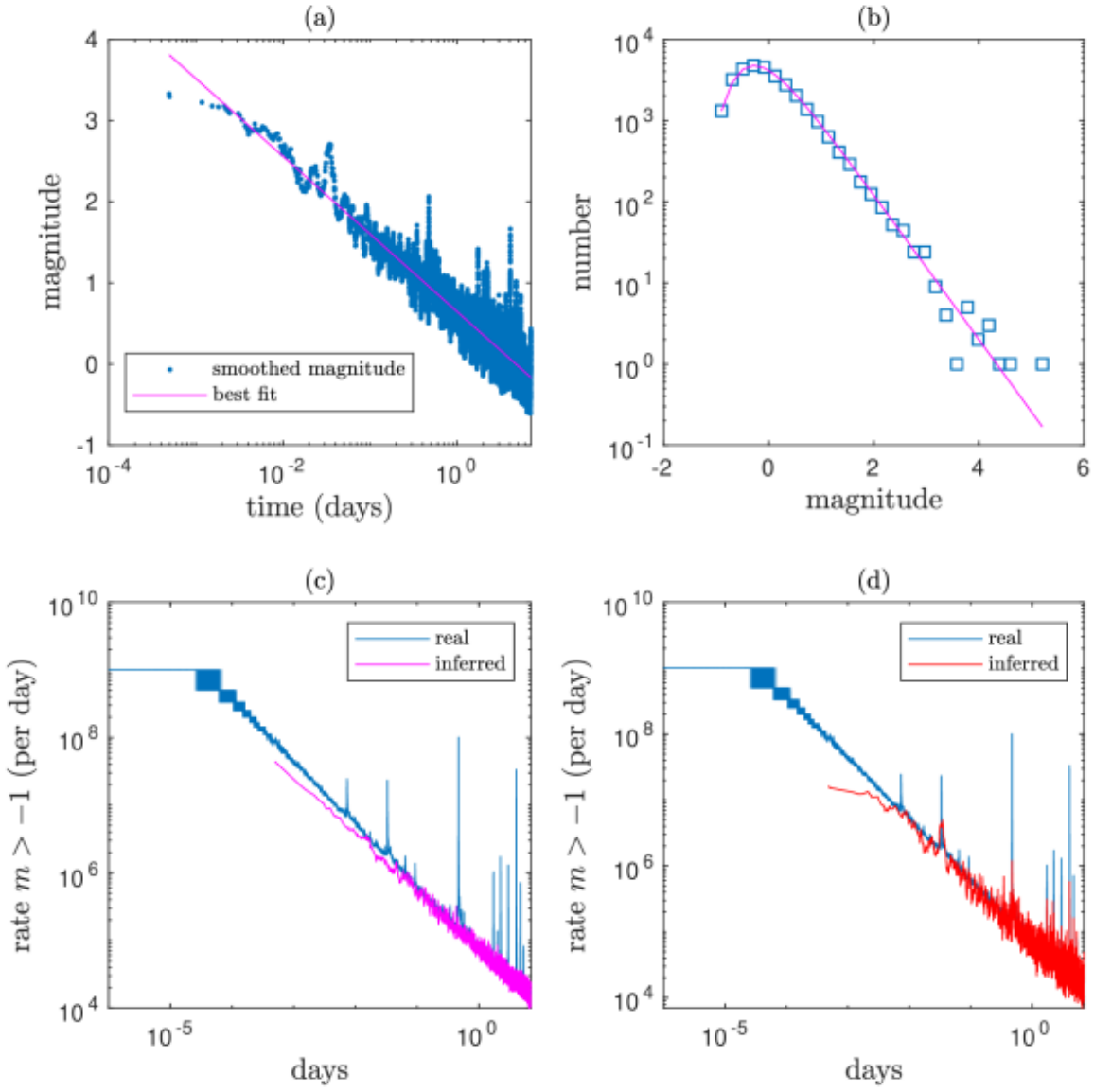

Figure S10: results from a synthetic catalog of earthquakes. (a) Magnitude vs time of the detected earthquakes. (b) Distribution of magnitude increments δm, with the best fit (Gutenberg-Richter times a Gumbel law) in magenta. (c) Inferred rate of earthquakes, compared to the true rate. (d) Same as (c), but directly using the smoothed magnitudes rather than the log-linear model, see text.

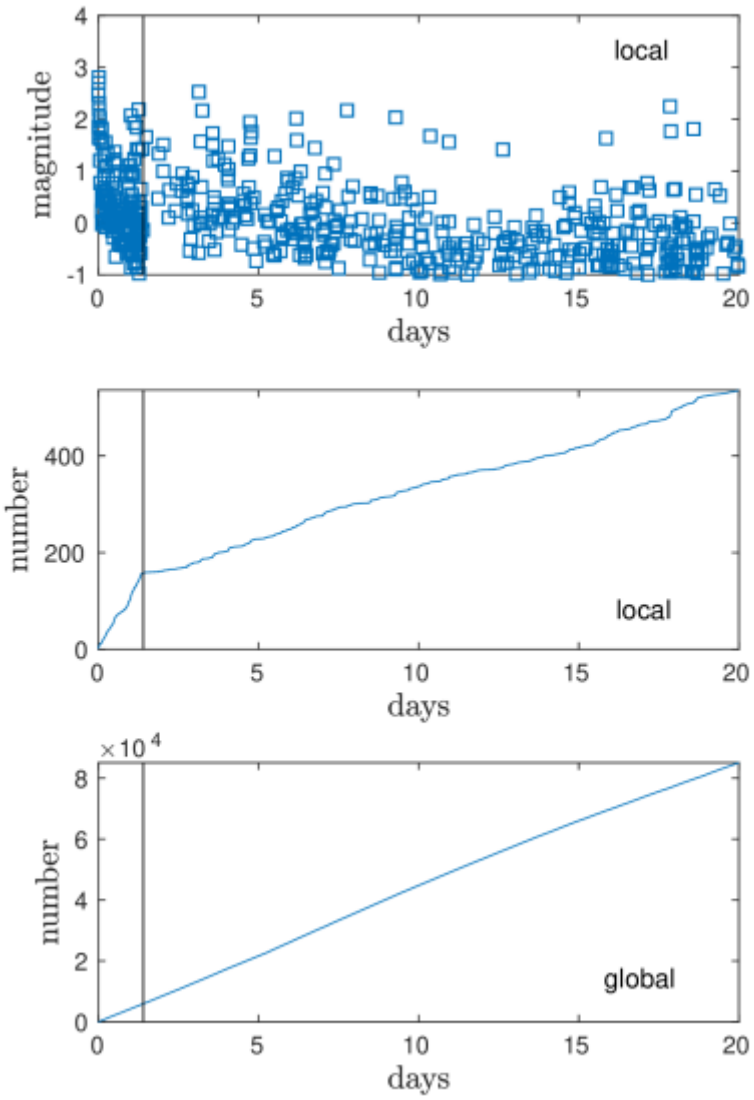

Figure S11: example of a local and global synthetic catalogs, with no true rate change at the time of the M7.1 mainshock (1.4 days, black vertical line). The apparent drop in rate for the local catalog is due to the increased activity after 1.4 days, and a lack of detection of small events, as directly seen on the top graph.

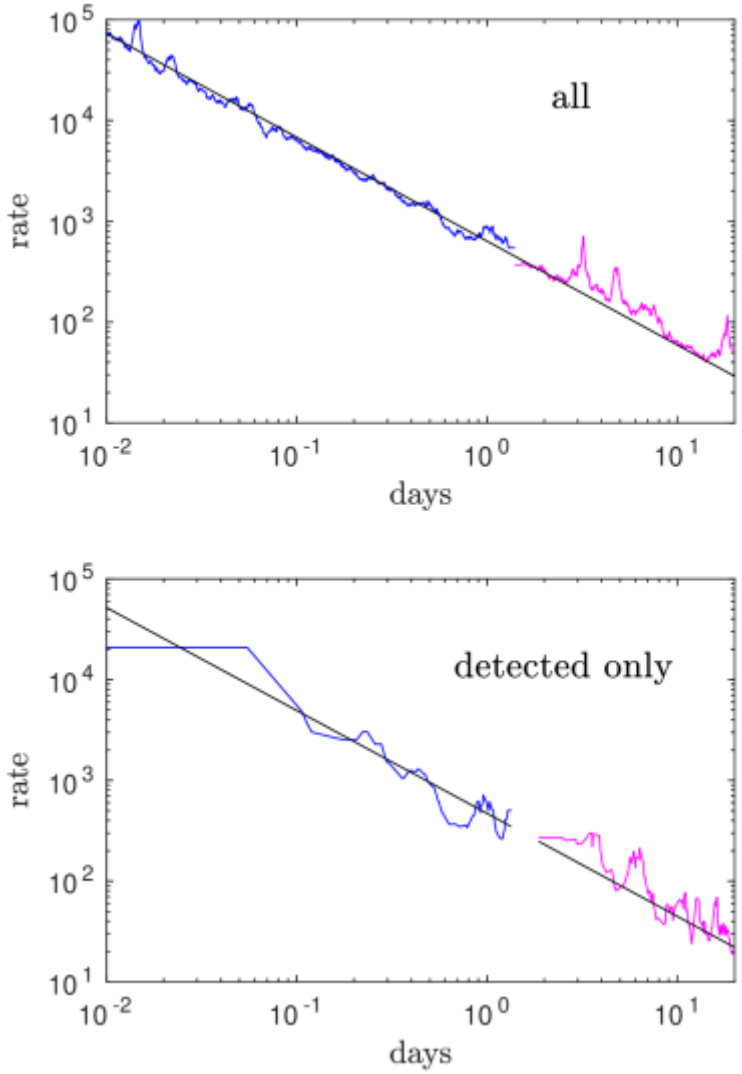

Figure S12: rate of earthquakes for the local synthetic catalog of Figure S11. The blue and magenta rates are for t<1.4 days and t>1.4 days, respectively. The best log-log linear fit (computed based on the t<1.4 day rate only) is in black. (Top) rate computed using all earthquakes, even those not detected; this gives the true rates. (Bottom) rate computed using only the detected earthquakes. The method is able to recover the true rate and the rate change with good accuracy.

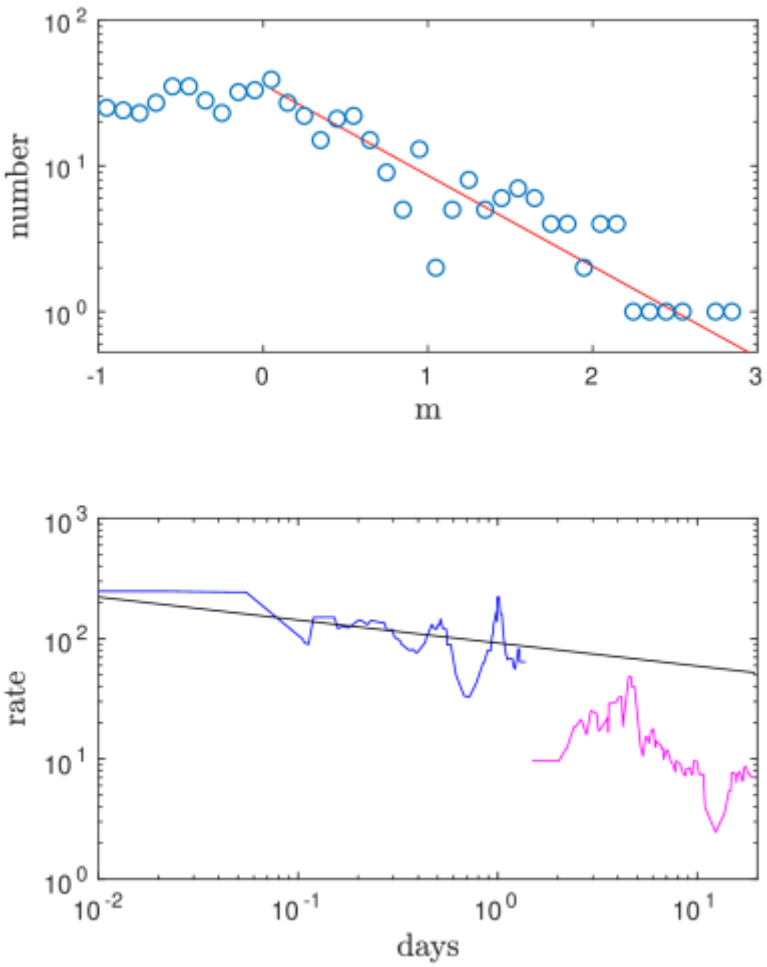

Figure S13: (top) number vs magnitude for the local detected catalog; a completeness magnitude $m_c=0$ and a b-value of 0.62 (red line) are found. (Bottom) rate of $m \geq m_c$ earthquakes, before (in blue) and after (in magenta) the 2nd mainshock at 1.4 days. The best log-log linear fit based on the t<1.4 days rate is shown in black. The rate change is estimated to $\rho=-0.94$.

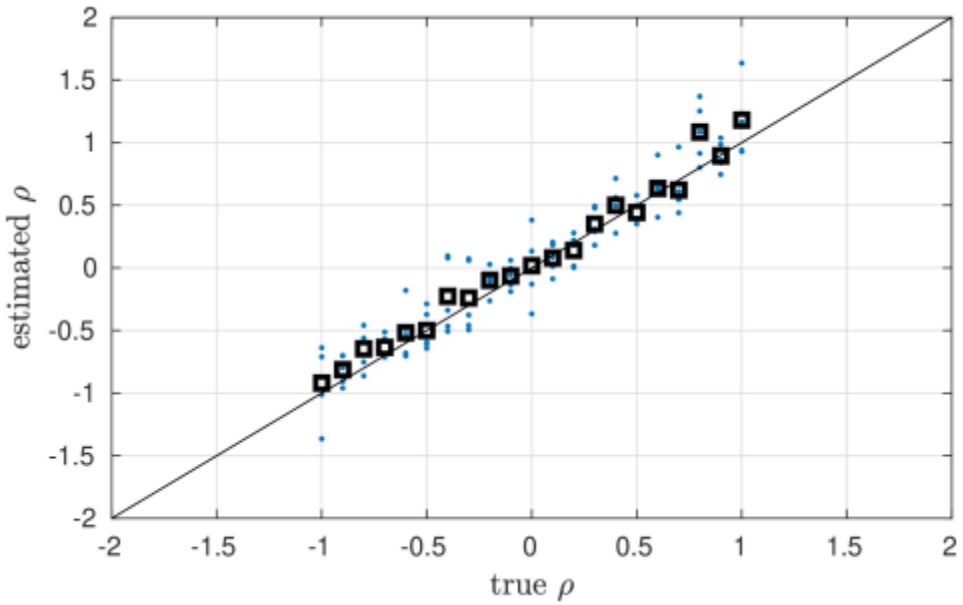

Figure S14: (blue) estimated vs true ρ values, for 100 synthetic (local) catalogs. We run 5 independent simulations for each value of the true ρ, which allows us to estimate the uncertainty $\Delta\rho=0.19$ of the estimated ρ. The black squares give the mean for the 5 realizations.

	SCSN only		SCSN + QTM	
location	ρ	v	ρ	v
A	0.14	0.11	-0.29	0.27
B	0.17	0.10	-0.77	0.19
C	1.00	0.14	0.72	0.18
D	1.02	0.15	0.81	0.27
E	0.19	0.07	-0.24	0.18
F	-1.10	0.29	-1.46	0.34

Table S1: rate change in log 10 scale (ρ) and normalized variance v of the best model, for the 6 locations A to F of Figures S5 and S6, for 0-7 days after the M7.1 mainshock. Columns 2 and 3 are for the SCSN catalog only (N=100 earthquake disks), and columns 4 and 5 are with the QTM earthquakes included (N=400 earthquake disks).